Original Article

DOI: 10.7860/JCDR/2026/88595.24374

Dentistry Section

Design, Physicochemical Characterisation, and Printability Optimisation of a Novel Composite Biomaterial Ink for Extrusion-based 3D Bioprinting: An In-vitro Study

PARKAVI ARUMUGAM[1], R SRIVARSAN[2], KAARTHIKEYAN GURUMOORTHY[3]

ABSTRACT

Introduction: Three-Dimensional (3D) bioprinting enables patient-specific regenerative strategies for improved oral health and quality of life, with rational Biomaterial Ink (BI) design being critical for extrusion-based printing as composition governs printability, structural fidelity, and biological relevance. Systematic optimisation is essential for developing BI suitable for oral and craniofacial tissue defects.

Aim: To develop a Polyethylene Glycol (PEG) - Polyethylene Glycol Diacrylate (PEGDA) -hydroxyapatite-collagen composite BI and to evaluate its feasibility for extrusion-based bioprinting through phase-wise printability assessment, followed by rheological and surface wettability characterisation.

Materials and Methods: The present in-vitro study was conducted at the Department of Biomaterials, Saveetha Dental College, Chennai, Tamil Nadu, India, from February 2023 to March 2023. BI formulations were sequentially developed by varying PEG, PEGDA, hydroxyapatite, and collagen concentrations. Phase-wise printability screening identified formulations with stable extrusion and shape retention. Selected formulations underwent rheological evaluation, printability assessment and surface wettability by contact angle analysis. Contact angle data were analysed using One-way Analysis of Variance (ANOVA) and Tukey's post-hoc test ($p<0.05$). Rheological analysis was performed qualitatively.

Results: Phase-wise optimisation identified BI-3 as exhibiting stable filament formation and favourable low-strain viscoelastic behaviour, supporting smooth extrusion and shape fidelity. Contact angle analysis revealed significant formulation-dependent differences in surface wettability ($p<0.001$).

Conclusion: The study successfully developed and optimised a composite BI for extrusion-based bone bioprinting, with BI-3 demonstrating the most favourable printability, rheological, and wettability characteristics, supporting its potential for alveolar bone bioprinting applications.

Keywords: Bone, Health, Periodontal disease, Regeneration, Three-dimensional

INTRODUCTION

Oral bone defects commonly arise from periodontal disease, oral pathologies, and trauma, often requiring regenerative intervention and rehabilitation [1]. Despite the use of advanced surgical materials and modalities such as guided bone regeneration, socket preservation, autografts, Bone Morphogenetic Proteins (BMP), enamel matrix derivatives, and platelet-derived growth factor, predictable bone regeneration remains challenging [2,3]. Consequently, advances in tissue engineering and regenerative medicine including 3D bioprinting, stem cell technologies, vascularisation strategies, decellularisation, recellularisation, smart biomaterials, organ-on-a-chip systems, and genetic engineering have emerged as promising approaches for restoring lost oral tissues [4].

3D bioprinting is an advanced tissue engineering approach that fabricates layer-by-layer scaffolds using bioinks composed of biomaterials, cells, and growth factors, enabling patient-specific constructs tailored to anatomical defects. Among current modalities-extrusion, inkjet, and laser-assisted [5] extrusion-based bioprinting is most prevalent due to its material versatility, scalability, customisability, and high cell viability [6]. BI are central to this process, governing structural integrity and functional performance while mimicking the native microenvironment; they may comprise biomaterials alone or include living cells [7]. Natural polymers provide biomimicry but limited mechanical strength, whereas synthetic polymers enhance stability and printability, necessitating precise rheological optimisation, as composition directly influences extrusion parameters and ultimately scaffold fidelity [8].

Collagen, abundant in the extracellular matrix, is widely used for its biocompatibility, bioactivity, tunable biodegradability, low immunogenicity, and hydrophilicity [9]. As bone's primary structural protein, it provides key biological and mechanical cues regulating cell behaviour [9,10]. Fish-derived type I collagen offers reduced zoonotic risk and greater ethical acceptance than mammalian sources [11], while promoting cell adhesion, proliferation, and differentiation via Arginine-Glycine-Aspartic acid (RGD) motifs Yamada S et al., 2014; Thirumalaivasan N, 2025; Yue C et al., 2024. It forms fibrillar hydrogels that mimic native extracellular matrix and support 3D cell growth [12-14], but limited thermal stability and mechanical strength necessitate crosslinking or blending with materials such as alginate, gelatin, or hydroxyapatite for improved printability and integrity.

Hydroxyapatite, a calcium phosphate material closely resembling the mineral phase of bone, is widely used in BI for 3D bioprinting of osseous scaffolds. Its excellent biocompatibility, osteoconductivity, and bioactivity support bone cell attachment, proliferation, mineralisation, and osteogenic differentiation via calcium and phosphate ion release, even in the absence of exogenous growth factors [15,16]. Incorporated as micro or nanoparticles, hydroxyapatite reinforces printed constructs and mimics native bone mechanics and biochemistry, improving suitability for load-bearing applications. Additionally, its affinity for bioactive molecules enables delivery of osteoinductive agents such as BMP-2. However, due to poor printability and brittleness in pure form, hydroxyapatite is typically blended with polymers such as alginate, gelatin, or PEG-based hydrogels to enhance extrusion and structural fidelity.

PEG is a synthetic, hydrophilic, biocompatible, non toxic, and non-immunogenic polymer used for cell and bioactive molecule encapsulation [17]. Its lack of intrinsic cell-adhesion sites is commonly overcome by RGD functionalisation [18]. Photo-crosslinkable derivatives such as PEGDA polymerise under Ultraviolet (UV) or visible light in the presence of photoinitiators (e.g., Irgacure 2959 or LAP), enabling rapid, spatially and temporally controlled scaffold formation [19]. This approach enhances structural integrity and allows tunable viscosity, mechanical properties, and degradation through molecular weight adjustment or material blending.

Despite extensive research on bone BI, many existing formulations either prioritise biological mimicry at the expense of printability or achieve adequate print fidelity through synthetic polymers while compromising biological relevance [20]. Although composite BI incorporating bone-mimetic components have been reported, there remains a need for studies that explicitly focus on feasibility, printability, and rheological optimisation for extrusion-based bioprinting in craniofacial bone regeneration. In response to this need, the present study aimed to develop a composite BI composed of PEG-PEGDA-hydroxyapatite-collagen, and to evaluate its feasibility for extrusion-based bioprinting through printability assessment, rheological characterisation, contact angle–based evaluation of surface hydrophilicity.

MATERIALS AND METHODS

The present in-vitro study was conducted at the Department of Biomaterials, Saveetha Dental College, Chennai, Tamil Nadu, India, from February 2023 to March 2023. The approval for the conduction of the study was obtained from the Institutional Scientific Review Board with the approval number SRB/SDC/PhD/PERIO-2264/23/TH-053. PEG 4000 and PEGDA, along with the photoinitiator system comprising Camphorquinone (CQ) and Ethyl 4-(Dimethylamino) Benzoate (EDMAB), and absolute ethanol were obtained from HiMedia Laboratories, India. Hydroxyapatite particulate graft (20-80 nm, 99.9% purity) was procured from Nano Research Lab, India, whereas marine fish collagen (95% extrapure grade) was purchased from Sisco Research Laboratories Pvt., Ltd., India. CELLINK Bio X bioprinter was used for bioprinting under sterile conditions.

As the present study was an in-vitro physicochemical evaluation, formal sample size calculation was not applicable; measurements were performed using technical replicates where relevant.

Study Procedure

Printability and contact angle analyses were performed in triplicate (n=3), consistent with standard biomaterials characterisation practices. Rheological measurements were conducted on a single representative sample (n=1) to obtain qualitative insight into viscoelastic behaviour from continuous sweep testing. Only freshly prepared BI formulations that were homogeneous, sterile, and adequately degassed were included for analysis. Samples exhibiting phase separation, visible aggregation, or air entrapment prior to testing were excluded to ensure consistency of physicochemical characterisation. All formulations meeting these criteria were subjected to printability assessment, and the outcomes were recorded as part of the evaluation. Rheological and contact angle measurements were performed on samples that satisfied basic handling and surface uniformity requirements to ensure reliable data acquisition.

BI development and evaluation were performed in a phased manner to assess suitability for extrusion-based 3D printing applications. Formulations were optimised through iterative compositional adjustments to obtain a homogeneous and extrudable system with appropriate handling characteristics. This was followed by sequential physicochemical characterisation, including printability assessment, rheological analysis, and contact angle measurement, to evaluate material performance. All analyses were conducted under standardised environmental conditions and uniform instrument settings to ensure consistency and reproducibility of results.

Development of Biomaterial Ink (BI): The composite BI comprised PEG, PEGDA, hydroxyapatite, and collagen as shown in [Table/Fig-1]. Varying concentrations of the components were evaluated in a phased manner for BI optimisation. BI formulations were prepared to a constant final volume of 10 mL. Solid constituents were weighed (mg) and liquid components were measured volumetrically (mL) prior to mixing. All formulations were expressed as percentage composition relative to the total final volume, thereby representing a standardised fixed-volume system.

The total solid content of the BI formulations was defined as the combined percentage of PEG, hydroxyapatite, and collagen relative to the final formulation volume, while PEGDA was considered the liquid phase. In the preliminary screening stage (Ink 1 to Ink 3), the total solid content ranged from 25% to 50% (w/v equivalent) based on variation in component ratios. In Phase II and Phase III, for BI-1 to BI-5, the total solid content ranged from 30% to 35%, whereas the Control BI (CB) exhibited a solid content of 24%. All formulations were prepared at a fixed final volume of 10 mL to ensure consistency and comparability across groups.

PEG 4000 flakes were first blended with PEGDA under controlled mild heating (40-50°C) to obtain a uniform polymeric matrix. Hydroxyapatite nanoparticles were subsequently incorporated into the mixture and homogenised using sonication to achieve uniform particle dispersion. Marine fish collagen powder was then added under refrigerated conditions (4-8°C) to preserve its structural integrity and prevent thermal denaturation. Separately, a photoinitiator solution was freshly prepared immediately prior to printing by dissolving CQ and EDMAB in absolute ethanol (20 mg CQ and 50 mg EDMAB in 100 µL ethanol) under light-protected conditions until a clear homogeneous solution was obtained. This photoinitiator solution was then slowly incorporated into each 10 mL batch of the composite BI under light-shielded conditions with continuous gentle stirring to ensure uniform distribution throughout the formulation.

Biomaterial Ink (BI) Optimisation: Optimisation was conducted in three phases: Phases I and II focused on identifying optimal PEGDA and PEG concentrations, while Phase III optimised hydroxyapatite and the bioactive component collagen.

- **Phase I: Identification of printable formulations through initial base composition screening**

Phase I involved identification of printable formulations through screening of different concentrations of the base polymer formulations, to identify the viscosity range that was conducive for printing and had the potential to be further modified. Three different concentrations of the polymeric components, with the addition of hydroxyapatite, were formulated in the following ratios:

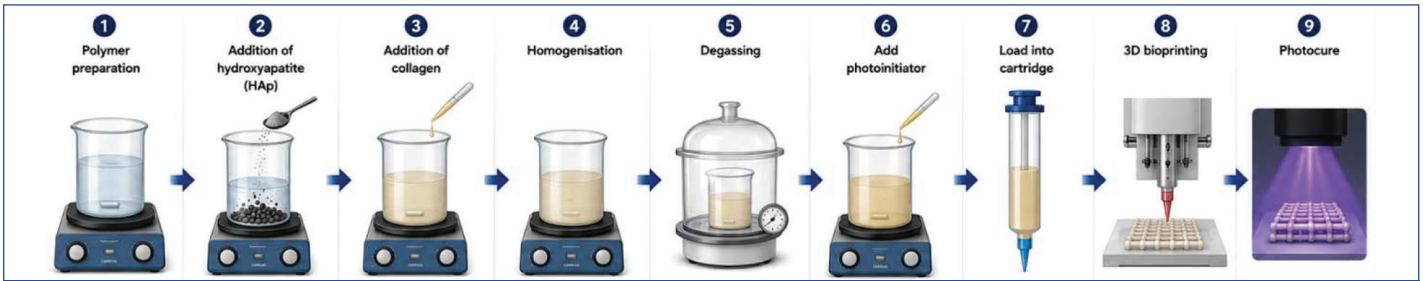

[Table/Fig-1]: Schematic representation of Biomaterial Ink (BI) development and 3d bioprinting process.

- Ink 1: PEGDA 50%, PEG 45%, hydroxyapatite 5%;
- Ink 2: PEGDA 70%, PEG 15%, hydroxyapatite 15%;
- Ink 3: PEGDA 75%, PEG 10%, hydroxyapatite 15%.

Three preliminary ink formulations with varying PEGDA, PEG, and hydroxyapatite concentrations were prepared as part of an empirical optimisation process. These formulations were screened for their suitability based on printability and overall handling characteristics. PEGDA was the primary crosslinkable base polymer and PEG and hydroxyapatite were adjusted proportionally to maintain formulation balance and modulate flow behaviour. These discrete compositions were selected to generate clearly distinguishable differences in flow characteristics during screening, rather than minor incremental changes. Preliminary extrudability was assessed using manual syringe-based extrusion based on the ability to produce a continuous, uniform filament without clogging or interruption, enabling identification of suitable formulations for further optimisation.

Among the three formulations, only Ink 2 showed potential for use as a BI. Although its viscosity required optimisation, Ink 2 enabled consistent filament extrusion and printability at 150-200 kPa at room temperature. Ink 1 was unsuitable due to excessive viscosity, requiring pressures >370 kPa and elevated temperature, while Ink 3, despite extruding at low pressure (60 kPa), was overly fluid and failed to maintain filament shape fidelity. Accordingly, Ink 2 was advanced to Phase II for further optimisation, and Ink 1 and Ink 3 were excluded from subsequent analyses.

- **Phase II: Identification of Optimal Polymeric Concentrations**

This phase assessed the effect of polymer concentration on BI printability. After incorporating marine collagen, optimal PEGDA-PEG ratios were identified to achieve suitable extrusion and shape fidelity and to enable Phase III optimisation. Accordingly, three BI formulations were prepared with fixed hydroxyapatite (14%) and collagen (1%) and varying PEGDA-PEG ratios.

- BI-1: PEGDA 70%, PEG 15%, hydroxyapatite 14%, collagen 1%
- BI-2: PEGDA 68%, PEG 17%, hydroxyapatite 14%, collagen 1%
- BI-3: PEGDA 65%, PEG 20%, hydroxyapatite 14%, collagen 1%

All formulations demonstrated acceptable printability; when printed using CELLINK Bio X bioprinter under sterile conditions at room temperature. However, BI-3 exhibited superior extrusion consistency and shape fidelity post-printing. Consequently, BI-3 was selected for further analysis of varying hydroxyapatite and collagen concentrations in Phase III.

- **Phase III: Identification of optimal hydroxyapatite and collagen concentrations**

BI-3 was further chosen for modifications of the concentrations of the osseous component and the biologic component of the BI. Three different formulations with different concentrations of hydroxyapatite and collagen, while maintaining the standardised concentrations of PEGDA at 65% and PEG at 20%, were prepared and analysed.

- BI-3: PEGDA 65%, PEG 20%, hydroxyapatite 14%, collagen 1%;
- BI-4: PEGDA 65%, PEG 20%, hydroxyapatite 13%, collagen 2%;
- BI-5: PEGDA 65%, PEG 20%, hydroxyapatite 11%, collagen 4%.

Based on the optimised PEGDA (65 wt%) and PEG (20 wt%) concentrations identified in Phase II, the remaining 15 wt% was apportioned between hydroxyapatite and collagen to generate three formulations (14:1, 13:2, and 11:4 wt% hydroxyapatite:collagen), enabling systematic fine-tuning of the hydroxyapatite-collagen ratio while maintaining constant polymer content and identifying the optimal composition for subsequent investigations. Phase II established the baseline formulation, following which hydroxyapatite (11-14 wt%) and collagen (1-4 wt%) were proportionally varied to refine matrix composition and optimise extrusion performance.

BI-5 was excluded due to poor filament formation, while BI-4 was printable but showed moderate shape fidelity. Overall, only three Phase II–III formulations exhibited suitable extrusion rheology and good post-print fidelity. BI-4 was retained despite moderate fidelity to assess the effects of hydroxyapatite and collagen variation on scaffold properties.

For the PEG-PEGDA-hydroxyapatite-collagen BI, a CB was formulated by omitting hydroxyapatite while retaining PEG, PEGDA, and collagen. The CB was derived from the formulation exhibiting the most favourable rheological properties (BI-3). To maintain a total composition of 100 wt%, the 14 wt% hydroxyapatite fraction was proportionally redistributed among PEGDA, PEG, and collagen using a scaling factor of 100/86 (≈1.16). The resulting theoretical concentrations (PEGDA 75.58 wt%, PEG 23.26 wt%, and collagen 1.16 wt%) were rounded to practical whole-number weight percentages (PEGDA 76 wt%, PEG 23 wt%, and collagen 1 wt%) for formulation. This ensured comparable rheological and printing behaviour, with hydroxyapatite as the sole variable. By preserving matrix composition, crosslinking behaviour, and collagen content, this design isolated the effect of hydroxyapatite, allowing any differences in biological outcomes to be attributed specifically to its presence. Based on this rationale, five printable formulations were selected for further characterisation and analysis.

- BI-1: PEGDA 70%, PEG 15%, hydroxyapatite 14%, collagen 1%;
- BI-2: PEGDA 68%, PEG 17%, hydroxyapatite 14%, collagen 1%;
- BI-3: PEGDA 65%, PEG 20%, hydroxyapatite 14%, collagen 1%;
- BI-4: PEGDA 65%, PEG 20%, hydroxyapatite 13%, collagen 2%;
- Control Biomaterial Ink (CB): PEGDA 76%, PEG 23%, collagen 1%.

Photoinitiator Preparation and Incorporation into BI

A fresh photoinitiator solution (20 mg CQ, 50 mg EDMAB in 100 µl ethanol) was prepared and 100 µl was added to each 10 mL BI batch to achieve 7 mg/mL total photoinitiator. The ~1% volume increase required no formulation adjustment, and partial ethanol evaporation minimised rheological effects. BI was kept under light-protected conditions until printing.

The photoinitiator solution was added uniformly to all formulations immediately prior to printing and was therefore treated as a constant processing additive rather than a variable compositional component. The nominal BI compositions (summing to 100%) reflect only the primary structural constituents (PEG, PEGDA, hydroxyapatite, and collagen), which were the variables under investigation. Although the inclusion of the photoinitiator results in a minor increase in total volume (~1%), its concentration was kept constant across all groups and thus does not affect the relative comparison between formulations. Given its low proportion and non-structural role (facilitating crosslinking without contributing to bulk matrix properties), it was excluded from the reported percentage composition for clarity and consistency with common practice in BI formulation studies. For transparency, the final BI can be considered to contain approximately 1% (v/v) photoinitiator solution in addition to the nominal 100% composition of the primary components.

Printability assessment served as the primary screening tool during phase-wise formulation development. Printability was assessed based on filament extrusion behaviour using the CELLINK bioprinter, specifically the ability to produce a continuous and uniform filament during extrusion without clogging or interruption, with extrusion

pressure adjusted as required for each formulation to enable consistent filament formation. Shape fidelity was not a primary outcome measure and was only qualitatively observed during printing, with attention to gross filament spreading, extrusion irregularities, and air bubble formation. No objective quantitative metrics (e.g., filament diameter, spreading ratio, or printability index) were applied, as this study was intended to identify formulations with suitable extrudability. Detailed rheological characterisation and surface wettability analysis (contact angle) were performed only for the optimised BI formulations demonstrating stable extrusion, and printability.

Tests of printability

The ability of the BI formulations for extrusion and filament formation was analysed in this printing stage. The pressure, temperature, feed rate, filament formation ability, and shape fidelity of the filaments were assessed in this phase. The CELLINK BIOX 3D bioprinter was utilised for the printing of the scaffolds. Two-layered grid scaffolds (20 mm × 20 mm × 1 mm) were fabricated using an 18-gauge nozzle at a printing speed of 3-4 mm/s with 50% infill density at room temperature, under sterile conditions. Extrusion pressure was adjusted for each formulation in accordance with its rheological behaviour to achieve stable and continuous filament deposition. The pressure ranges applied were 17-22 kPa for BI-1, 25-39 kPa for BI-2, 14-19 kPa for BI-3, 17-22 kPa for BI-4, and 17-24 kPa for CB. Following fabrication, the 3D-bioprinted scaffolds were photo-crosslinked using blue light (460 nm) and subsequently maintained under appropriate conditions for further evaluation. Post-printing, the 3D-bioprinted scaffolds were photo-crosslinked using a dental Light Emitting Diode (LED) light-curing unit emitting blue light (~460 nm). Each construct was exposed for 60 seconds at a working distance of approximately 1-2 cm from the light source. The unit delivers a light intensity of approximately 1200-2000 mW/cm^2, as specified by the manufacturer. All samples were cured under identical conditions to ensure uniform crosslinking.

Rheologic analysis

Rheology was assessed using a Malvern Bohlin Gemini II Rheometer. Sterile, degassed BI samples (0.5-2 mL) were analysed in the pre-crosslinked state using a parallel plate geometry with a gap of 0.5-1 mm at 25°C. Prior to measurement, samples were carefully loaded onto the lower plate to minimise air entrapment, excess material was trimmed, and the samples were allowed to equilibrate for 2-3 minutes before testing. Measurements were conducted promptly to minimise dehydration effects. Flow sweeps (0.01-1000 s^{-1}) evaluated shear-thinning, followed by amplitude sweeps (1 Hz, 0.01-100% strain) to define the Linear Viscoelastic Region (LVR) and frequency sweeps within the LVR (0.1-100 rad/s) to measure storage (G′) and loss (G″) moduli. Rheological measurements were conducted to provide a qualitative and comparative assessment of printability-related properties, and therefore emphasis was placed on overall trends rather than statistical comparison.

Contact angle analysis

Contact angle analysis was performed using the sessile drop method on an Ossila Contact Angle Goniometer. Light-cured BI samples were prepared as thin, uniform films on glass slides, as shown in [Table/Fig-2]; although the exact thickness was not measured, consistent spreading conditions were maintained across all samples. Prior to sample deposition, glass substrates were thoroughly cleaned with ethanol rinse and air-dried, to ensure a contaminant-free and hydrophilic surface. A droplet (2-5 µL) of distilled water was placed on the sample surface and allowed to stabilise for 5-10 seconds before imaging. Contact angles were determined using tangent fitting on both sides of the droplet and averaged. Contact angle measurements were performed on three independent samples per group (n=3), each prepared and cured separately. For each sample, measurements were obtained at three different locations per sample at room temperature (~25°C, ~50% RH) and reported as mean±Standard Deviation (SD). The use of glass slides as the substrate provided a smooth, flat, and reproducible surface, minimising variability and enabling consistent comparison of wettability across different formulations.

STATISTICAL ANALYSIS

Statistical analysis was performed only for contact angle measurements, as these represent discrete quantitative data. Rheological parameters were evaluated based on overall trends consistent with the proof-of-concept design; therefore, statistical analysis was not performed, as the focus was on qualitative assessment of flow and viscoelastic behaviour. Normality of contact angle data was assessed using the Shapiro-Wilk test, and all groups demonstrated a normal distribution ($p>0.05$). Homogeneity of variances was confirmed using Levene's test ($p=0.063$). Accordingly, contact angle values were analysed using One-way ANOVA followed by Tukey's post-hoc test. A p-value <0.05 was considered statistically significant.

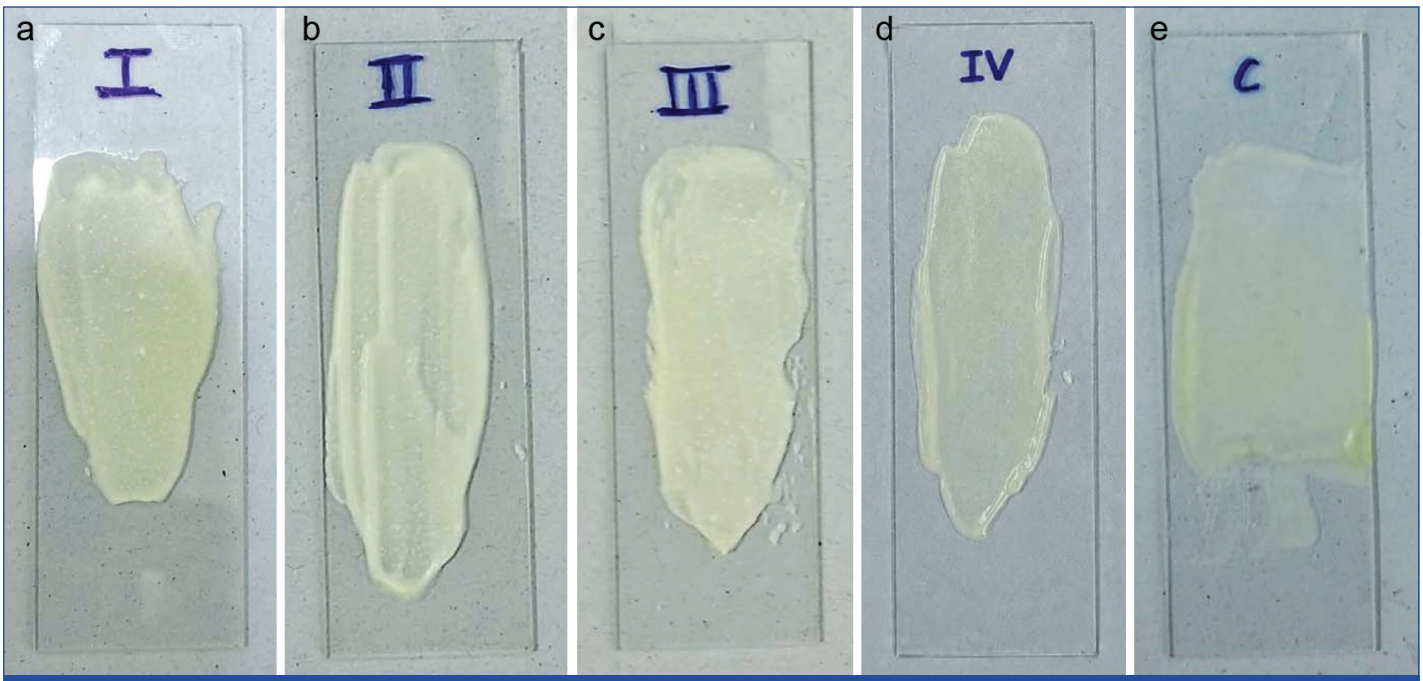

[Table/Fig-2]: Biomaterial Ink (BI) smears for surface wettability assessment: a) BI-1; b) BI-2; c) BI-3; d) BI-4; e) CB.

RESULTS

Tests of printability

Printability was primarily evaluated based on the ability of the BI to achieve continuous and stable filament extrusion under defined printing conditions. Constructs were visually assessed based on predefined criteria, including filament continuity, extrusion uniformity, and the presence of discontinuities, filament breakage, or spreading. While the ability to preserve the intended grid architecture, as well as strand definition and pore formation, was also observed, these were considered supportive indicators rather than primary endpoints. Constructs exhibiting continuous filament deposition with minimal disruption and spreading were regarded as printable. Representative scaffold images were examined to support the assessment of filament formation, uniformity, and overall structural integrity. For classification purposes, shape fidelity was qualitatively defined based on the preservation of filament architecture and pore structure, where constructs showing well-defined, continuous filaments with minimal spreading and clearly distinguishable pores were considered to have good shape fidelity, whereas those exhibiting filament merging, irregular strand morphology, or pore collapse were classified as having poor shape fidelity.

Printability was evaluated for formulations developed across Phases I-III [Table/Fig-3,4]. Phase I identified a base ink suitable for extrusion, with Ink 2 exhibiting continuous filament formation at moderate pressure and room temperature, along with superior post-print shape fidelity, thereby defining PEGDA (70%) and PEG (15%) as optimal extrusion ranges. Phase II incorporated all components to optimise polymer concentrations, with all BI showing acceptable printability and BI-3 demonstrating the highest print resolution and shape fidelity. The extrusion pressure of all BI scaled with viscosity, primarily governed by polymer content. In Phase III, BI-3 was further optimised by varying hydroxyapatite and collagen while fixing PEGDA (65%) and PEG (20%), revealing high sensitivity of printability to bioactive loading, where increased collagen and suboptimal mineral–collagen ratios impaired filament continuity and shape fidelity. Overall, this phase-wise strategy enabled progression from extrusion feasibility to enhanced dimensional stability, culminating in an optimised BI exhibiting stable extrusion, high print resolution, and improved scaffold structural fidelity.

Rheologic analysis

Consistent with phase-wise printability results, comparative rheological analysis of the selected formulations [Table/Fig-5,6] revealed distinct flow and viscoelastic profiles that mechanistically explained extrusion performance and post-print stability. BI-1 exhibited classical shear-thinning behaviour, with viscosity decreasing as a function of increasing shear rate (s^{-1}), and demonstrated elastic dominance (G´>G˝) within the low-strain (%)LVR, enabling smooth extrusion but only moderate shape fidelity due to limited elastic recovery. BI-2 showed stronger elastic dominance within the LVR and improved shape retention, although minor fluctuations at higher shear rates may have contributed to slight extrusion non-uniformity. BI-3 combined a high storage modulus (G´) at low strain, controlled shear-thinning with increasing shear rate, and behaviour indicative of improved structural recovery, accounting for its enhanced extrusion stability, shape fidelity, and structural integrity. BI-4 demonstrated acceptable shear-thinning behaviour and extrusion performance but reduced elastic recovery, consistent with moderate post-print stability, while the control bioink exhibited viscosity-dominated behaviour (G˝≥G´) with weak elasticity, resulting in poor filament formation and printability. Overall, the rheological profile of BI-3 closely aligned with the observed printability trends, identifying it as the most suitable formulation for extrusion-based bioprinting in this study. For clarity, viscosity is expressed as a function of shear rate (s^{-1}), while viscoelastic properties (G´ and G˝) are interpreted based on shear strain (%) and angular frequency (rad/s).

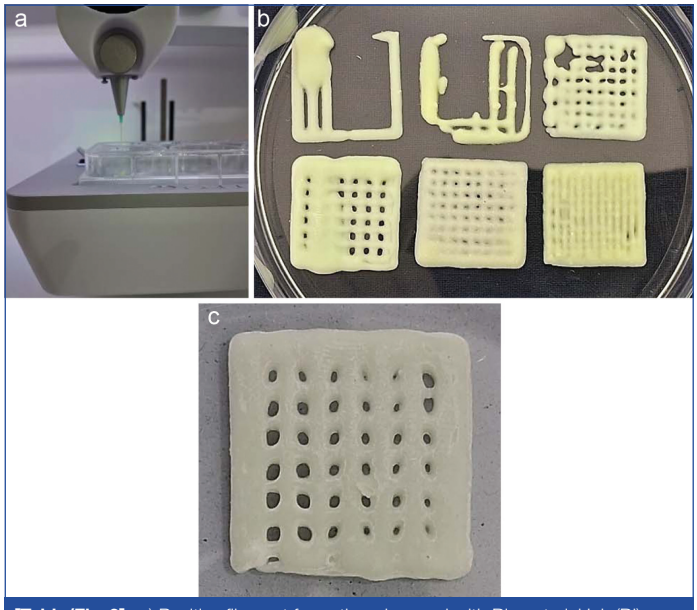

[Table/Fig-3]: a) Positive filament formation observed with Biomaterial Ink (BI) on extrusion; b) Image showing different stages of printability optimisation of bioink; c) Scaffold printed with an optimised Biomaterial Ink (BI) formulation.

Contact angle analysis: Contact angle analysis [Table/Fig-7,8] was conducted to evaluate surface wettability of the BI formulations. Contact angle measurements were performed in triplicate (n=3) for each group, with measurements obtained at three independent locations per sample, and reported as mean±standard deviation. Mean contact angles differed significantly among formulations (ANOVA: $F=2452.689$, $p<0.001$). The large effect size observed may be influenced by the low within-group variability, which in turn reflects the use of automated image-based measurement and limited number of independent replicates. BI-1 showed the lowest contact angle (17.09±0.08°), indicating the highest hydrophilicity, followed by BI-3 (19.36±0.43°). BI-4 exhibited moderate wettability (24.16±0.31°), while the control (27.06±0.30°) and BI-2 (37.16±0.08°) were less hydrophilic, with BI-2 showing the highest contact angle. Each contact angle value represents the average obtained from automated frame-based measurements of a single sessile droplet, and three such measurements were performed per sample. Tukey's post-hoc analysis [Table/Fig-9] confirmed significant differences among all formulations ($p<0.001$). Overall, BI-1 and BI-3 demonstrated superior hydrophilicity, which may favour cell attachment and proliferation in tissue engineering applications.

Interestingly, BI-2 exhibited a comparatively higher contact angle despite having an intermediate composition relative to BI-1 and BI-3, indicating the absence of a linear relationship between composition and wettability. This behaviour suggests that surface properties may be influenced by factors beyond bulk composition, such as polymer chain organisation, phase distribution, and crosslinking density. It is possible that the specific PEG-PEGDA ratio in BI-2 promotes altered surface presentation of hydrophilic groups or differences in network structure following photopolymerisation, thereby affecting surface energy. These findings highlight the complexity of wettability in multi-component hydrogel systems and suggest that further surface-specific characterisation would be required to fully elucidate the underlying mechanisms. Therefore, contact angle values should be interpreted as formulation-specific outcomes rather than strictly composition-dependent trends.

DISCUSSION

The foremost step in BI design is the selection of compatible components with complementary behaviour that collectively provide biomimetic cues relevant to the target tissue [20]. A composite formulation strategy was employed to balance biological functionality and printability, using components with inherent biocompatibility,

Phase	Biomaterial Ink (BI)	Pressure (kPa)	Temperature (°C)	Speed (mm/sec)	Nozzle gauge	Extrusion	Filament formation	Shape fidelity
Phase I	Ink 1	> 370	35 - 40	NA	18 gauge (green)	Negative	Negative	NA
	Ink 2	150-200	RT	2	18 gauge (green)	Positive	Positive	Good
	Ink 3	60-70	RT	3	18 gauge (green)	Positive	Positive	Poor
Phase II	Biomaterial Ink 1	17-22	RT	3	18 gauge (green)	Positive	Positive	Good
	Biomaterial Ink 2	25-39	RT	3.5	18 gauge (green)	Positive	Positive	Good
	Biomaterial Ink 3	14-19	RT	4	18 gauge (green)	Positive	Positive	Good
Phase III	Biomaterial Ink 4	7	RT	6	18 gauge (green)	Positive	Positive	Average
	Biomaterial Ink 5	20	RT	6	18 gauge (green)	Positive	Negative	Poor
	Control Biomaterial ink	4	RT	6	18 gauge (green)	Positive	Positive	Poor

[Table/Fig-4]: Printability parameters of the formulations (RT: Room temperature, NA: Not applicable).

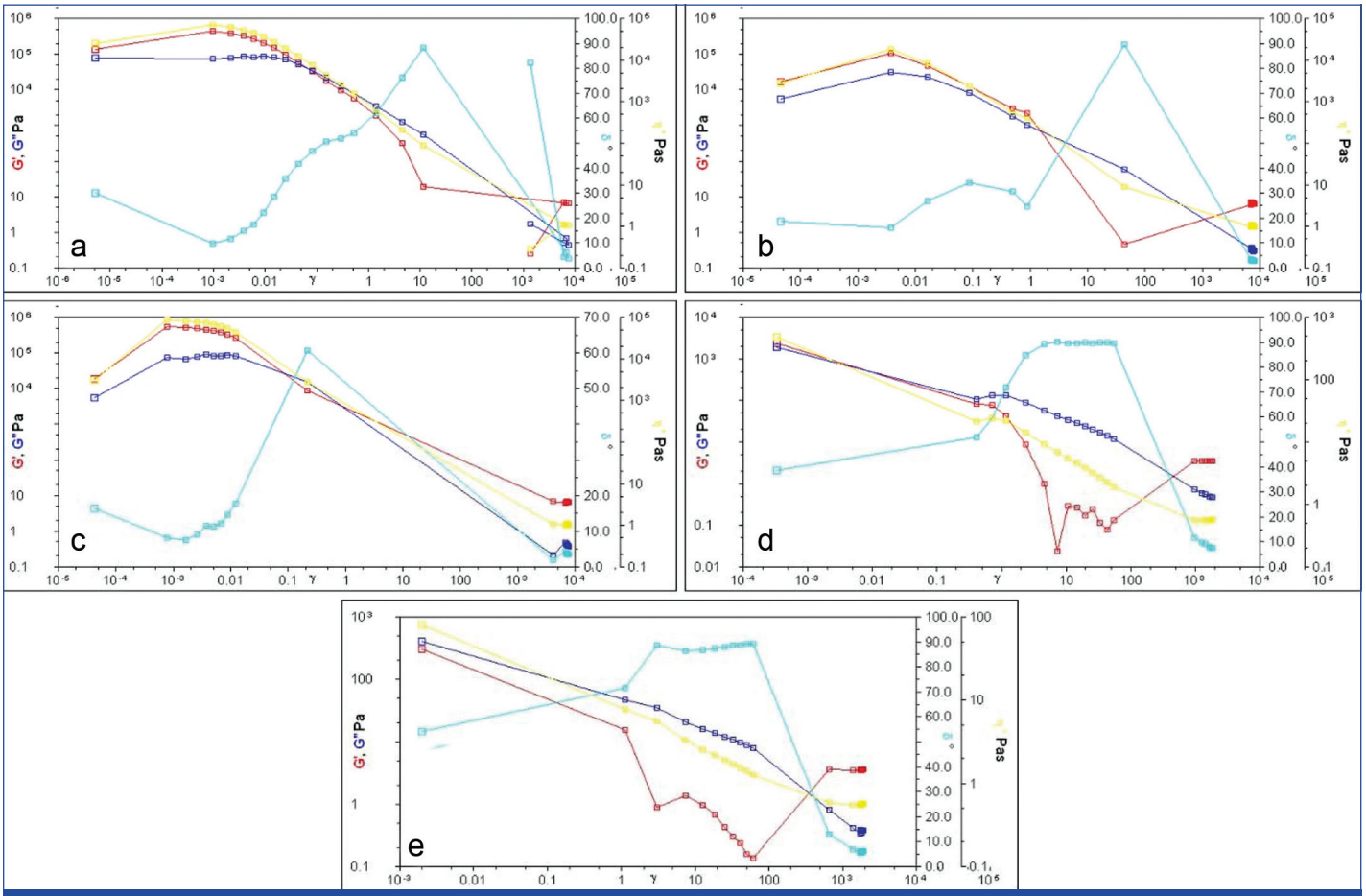

[Table/Fig-5]: Rheologic characterisation of different biomaterial ink formulation: a) BI-1; b) BI-2; c) BI-3; d) BI-4; e) CB; Red curve represents the storage modulus (G′), blue curve represents the loss modulus (G″), yellow curve represents the complex viscosity (η*), and cyan curve represents the phase angle (δ).

Rheologic parameter	Biomaterial ink I	Biomaterial ink II	Biomaterial ink III	Biomaterial ink IV	Control biomaterial ink
Viscosity (yellow-η*)	High at low shear rate; steady decrease with increasing shear rate (classic shear-thinning)	High at low shear; decreases with some irregularities	Peaks around $\gamma = 0.01\ s^{-1}$, then sharply decreases (complex shear-thinning)	Viscosity decreases with increasing shear strain, indicating pronounced shear-thinning behaviour	High at low shear; decreases steadily with increasing shear strain, indicating shear-thinning but at lower viscosity levels
Storage modulus (RED-G′)	High and stable at low γ; decreases with increasing γ	Peaks early; decreases sharply after $\gamma \approx 0.1\ s^{-1}$; slight increase at high γ	Very high peak at low γ; decreases steadily, remains dominant	Moderate at low γ; decreases sharply at mid γ with partial recovery at higher γ	Lower G′ at low γ; decreases markedly with increasing γ, indicating weak elastic network
Loss modulus (Blue-G″)	Lower than G′ throughout; follows similar downward trend	Increases initially; remains below G′; small spike at high γ	Mirrors G′ with a peak at low γ; lower than G′ at all points	Comparable to G′ at low γ; decreases gradually with increasing shear strain	Comparable to or exceeds G′ at mid-to-high γ, reflecting dominant viscous behaviour
Phase angle (CYAN-δ)	Low at low γ; increases with shear (transition to viscous behaviour)	Low and steady at low γ; sharp increase around mid shear rates	Low at low γ; peaks at mid γ, then decreases-showing viscoelastic transition	Increases with shear strain, indicating a transition toward viscous-dominated behaviour	High phase angle at mid γ followed by sharp decrease at high γ, indicating unstable viscoelastic transition
Elastic vs viscous nature	Predominantly elastic at low γ; becomes more viscous at higher γ	Elastic-dominant throughout with brief viscous transition	Strongly elastic at low γ with a transient viscoelastic shift	Elastic-dominant at low γ with a clear shift to viscous behaviour at higher γ	Predominantly viscous with limited elastic dominance
Shear thinning behaviour	Pronounced and smooth	Present but less uniform	Highly responsive with distinct transition point	Strong and well-defined, suitable for extrusion-based printing	Present but less pronounced and less controlled

Printability (extrusion)	Smooth due to shear-thinning	Smooth but slight inconsistencies at high shear	Excellent due to complex but controlled shear-thinning	Good; facilitated by reduced viscosity and viscous dominance at higher shear	Limited; low elastic support may affect filament continuity
Shape fidelity (post-print)	Good due to dominant G′	Very good; retains structure well	Excellent; high G′ ensures structural integrity	Moderate; elastic recovery supports shape retention	Poor to moderate; insufficient G′ leads to spreading
Overall structural integrity	High	Very High	Superior	Moderate to high	Low to moderate

[Table/Fig-6]: Rheological analysis of biomaterial ink formulations as a function of shear strain (γ).

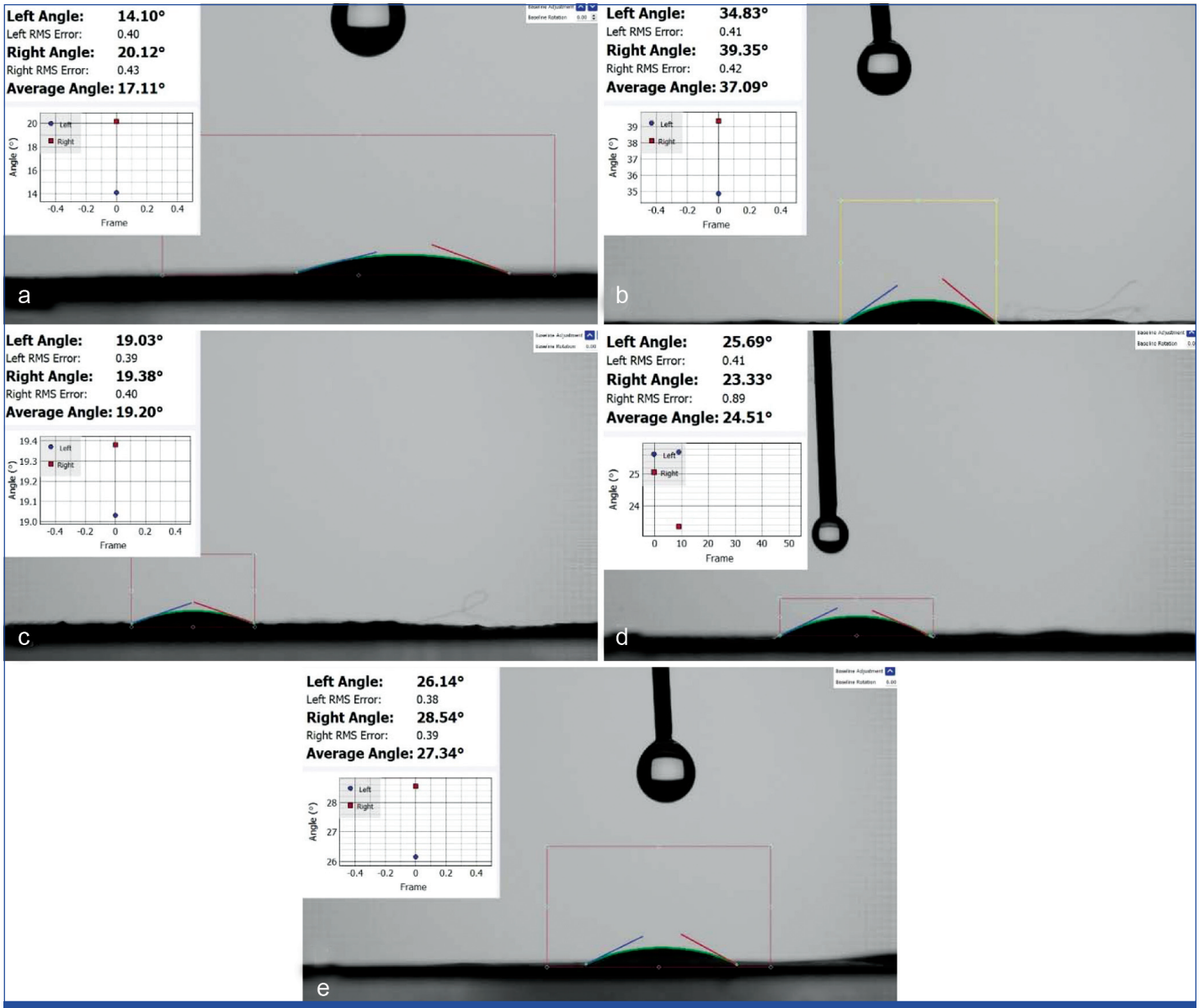

[Table/Fig-7]: Contact angle analysis of different biomaterial ink formulations: a) BI-1; b) BI-2; c) BI-3; d) BI-4; e) CB.

Bioink	Mean contact angle	Std. dev	f-value	p-value	df (between, within)	Effect size (η^2)
BI-1	17.0867	0.07767	2452.689	<0.001	(4, 10)	0.999
BI-2	37.1633	0.08083				
BI-3	19.3633	0.42899				
BI-4	24.1567	0.30665				
CB	27.0567	0.29569				

[Table/Fig-8]: One-way ANOVA analysis of contact angle values of biomaterial ink formulations.

Groups		Mean difference (I-J)	Sig.	95% Confidence interval	
				Lower bound	Upper bound
BI-1	BI-2	-20.076*	<0.001	-20.815	-19.337
	BI-3	-2.276*	<0.001	-3.015	-1.537
	BI-4	-7.070*	<0.001	-7.808	-6.331
	CB	-9.970*	<0.001	-10.708	-9.231
BI-2	BI-3	17.800*	<0.001	17.061	18.538
	BI-4	13.006*	<0.001	12.267	13.745
	CB	10.106*	<0.001	9.367	10.845
BI-3	BI-4	-4.793*	<0.001	-5.532	-4.054
	CB	-7.693*	<0.001	-8.432	-6.954
BI-4	CB	-2.900*	<0.001	-3.638	-2.161

[Table/Fig-9]: Tukey's Post-hoc analysis of contact angle values of biomaterial ink formulations.

biodegradability, hydrophilicity, and crosslinkability. Hydroxyapatite and collagen were incorporated to replicate the mineral and organic phases of bone, respectively.

Rheology was dictated by polymer structure and molecular weight [21] with PEGDA and PEG 4000 enabling viscosity control through concentration variation. PEGDA-PEG-hydroxyapatite base inks

were screened in Phase I for printability. Phase II introduced collagen and optimised polymer ratios to improve rheology and fidelity, while Phase III further adjusted hydroxyapatite and collagen to enhance biological relevance. Although the sole addition beyond Phase I, collagen conferred biofunctionality and altered rheology. Optimised formulations were subsequently evaluated for combined effects on scaffold performance.

Printability was evaluated across all phases as a screening tool, while detailed rheological characterisation was limited to the final optimised BI formulations. This allowed rheology to mechanistically explain phase-wise printability trends rather than act as a predictive filter [22]. Linking flow behaviour with extrusion stability, filament formation, and shape fidelity clarified the influence of molecular structure, molecular weight, and component concentration on BI performance.

In Phase I, higher PEG 4000 and lower PEGDA contents increased viscosity, requiring higher extrusion pressure and temperature and frequently causing nozzle clogging due to reduced extrusion stability, attributed to the high molecular weight and crystalline nature of PEG 4000 [23,24]. Conversely, PEGDA-rich formulations extruded easily but showed poor post-print shape fidelity owing to inadequate structural integrity. Phases II and III demonstrated that printability is confined to a narrow compositional window, with even small collagen variations (1-2%) markedly affecting extrudability, print resolution, and shape fidelity, highlighting the sensitivity of the system to bioactive loading.

PEG-based bone BI, such as Oligo(poly(ethylene glycol) fumarate) (OPF)-gelatin systems, exhibit printability only within a narrow compositional window, with optimal extrusion at ~15 wt% OPF and ~5 wt% gelatin; lower gelatin yields fluid inks, while higher levels cause excessive stiffness and poor extrusion [25]. This closely mirrors the present results, where phase-wise compositional control governed extrusion stability and shape fidelity, emphasising the need for systematic formulation optimisation in osseous BI design [25].

The rheological trends supported the phase-wise printability outcomes, highlighting viscoelastic balance as a key determinant of extrusion performance and post-print stability. Formulations lacking sufficient elastic recovery or exhibiting viscous dominance showed compromised structural integrity, whereas balanced shear-thinning behaviour and elastic response enabled stable multilayer deposition. These observations emphasise that effective BI design requires coordinated tuning of flow and recovery properties rather than shear-thinning behaviour alone. The rheological behaviour showed a predictive association with printability outcomes, rather than a defined mechanistic relationship. Rheological characterisation thus served as a comparative predictive indicator of extrusion behaviour, supported by qualitative print fidelity assessments under standardised conditions.

A recent study employed a multiple linear regression model to predict the viscosity of 23 formulations comprising alginate, carboxymethyl cellulose, and oxidised nano-fibrillated cellulose, based on 483 measurements across 21 shear rates, demonstrating that viscosity is strongly influenced by both component ratios and shear rate, with comparable viscosity values achievable across formulations with varying solid contents [26]. The present study similarly highlights the role of compositional tuning and shear-dependent behaviour in governing rheological response. In line with previous reports, double-network hydrogel systems combining gellan gum and PEGDA have demonstrated that integrating shear-thinning behaviour with rapid UV crosslinking enables the fabrication of shape-retentive and structurally stable constructs, while maintaining high cell viability (>87%) over extended culture periods [27]. Such findings underscore the importance of coupling rheological optimisation with post-print stabilisation strategies to achieve functional 3D bioprinted constructs.

Mineral reinforcement with hydroxyapatite increases BI viscosity and elastic modulus, improving extrusion stability and shape fidelity [28]. Optimal printability has been reported at moderate hydroxyapatite contents (1-5 wt%), while higher loading disrupts the viscous-elastic balance required for stable filament formation and reduces print fidelity [29]. The relatively higher hydroxyapatite content (~11-15% w/v), compared to commonly reported literature values (1-5 wt%), was incorporated to enhance scaffold mechanical stability, mineral phase reinforcement, and osteoconductive performance required for structural support in cranial defect models, in contrast to low-solid-content hydrogel systems primarily optimised for cell encapsulation and injectability. Likewise, collagen fibrillogenesis governs BI gelation and rheology, with low-density formulations (<5-10 mg/mL) extruding easily but lacking structural fidelity, and high-density BI (>20 mg/mL) better retaining 3D shape yet posing printability and cell-viability challenges, underscoring the strong composition dependence of BI performance [30,31].

Surface wettability, as assessed by contact angle analysis, demonstrated significant variation among the developed BI. BI-1 and BI-3 exhibited markedly lower contact angles compared to the control and other formulations, indicating enhanced hydrophilicity, which is generally favourable for protein adsorption and subsequent cell adhesion in tissue engineering applications. In contrast, BI-2 showed a comparatively higher contact angle despite its intermediate compositional profile, suggesting that wettability was not solely governed by bulk formulation ratios. This non-linear behaviour indicates that surface properties in composite systems with similar properties are likely influenced by additional factors such as polymer chain organisation, phase distribution, and crosslinking density induced during photopolymerisation. The observed variation highlights that surface energy in multi-component hydrogel systems is a complex, emergent property rather than a direct function of composition alone. Accordingly, contact angle measurements reflect formulation-dependent physicochemical outcomes arising from component interactions rather than bulk composition alone, and further surface-oriented characterisation would be required to better elucidate the structural determinants governing wettability in these BI systems.

Surface wettability influences extrusion and early biointeractions. Contact angle analysis showed all optimised BI were highly hydrophilic and suitable for extrusion-based osseous applications. Despite significant differences ($p<0.05$), no consistent compositional trend was observed; and pairwise data are provided as supplementary material. High wettability likely enhances filament fusion and early protein and cell interactions, supporting the rheological and printability findings.

Rational BI design underpins extrusion-based bioprinting, as polymer-filler-crosslinker interactions control rheology, filament stability, and structural integrity [32]. For craniofacial and oral bone applications, BI must balance mechanical support, biological compatibility, and geometric precision [33]. Accordingly, incorporation of hydroxyapatite and collagen into a PEG-PEGDA matrix provides compositional biomimicry and, with optimised rheological properties, may facilitate the fabrication of stable, defect-specific constructs, which warrant further in-vitro and in-vivo evaluation for potential applications in alveolar and craniofacial regeneration.

Unlike studies that empirically screen multiple formulations, this study employed a rationale-driven optimisation approach, iteratively refining polymer concentrations using predefined printability criteria, thereby establishing rheology-guided design as a prerequisite for craniofacial bone bioprinting.

Limitation(s)

The present study has several limitations that should be acknowledged. First, it was designed as a proof-of-concept

investigation and lacked in-vitro or in-vivo biological validation, limiting direct interpretation of clinical applicability. Second, rheological parameters were interpreted qualitatively without statistical analysis, restricting quantitative comparison between formulations. Third, printability assessment was based on predefined visual criteria rather than quantitative image-based metrics. Additionally, while contact angle measurements were performed under controlled conditions, detailed surface characterisation was not undertaken, which may limit comprehensive interpretation of wettability behaviour. Potential confounding factors such as minor variations during the printing process and environmental parameters were minimised through standardised protocols but cannot be entirely excluded. Further studies incorporating quantitative, physicochemical, mechanical, surface, and biological, including cellular response, long-term stability, and osteogenic performance are required to validate these findings. Nevertheless, the phase-wise design framework established here provides a robust foundation for future cell-laden bioprinting and translational craniofacial bone tissue engineering applications.

CONCLUSION(S)

This study presents a systematically optimised PEG-PEGDA-hydroxyapatite-collagen BI for extrusion-based 3D bioprinting. The formulation demonstrated favourable shear-thinning behaviour, printability, and surface wettability, indicating its suitability for stable extrusion and scaffold fabrication. Although the study is limited to physicochemical characterisation and printability assessment, the results establish a robust material platform for further investigation. Future studies incorporating detailed mechanical characterisation, cytocompatibility, osteogenic potential, and in-vivo evaluation are required to validate its applicability for craniofacial and alveolar bone tissue engineering.

Data availability statement: The datasets analysed during the current study are available from the corresponding author upon reasonable request.

Authors' contribution: All authors contributed to the conception and design of the study, data acquisition and analysis, manuscript drafting and critical revision, and approved the final version of the manuscript.

Artificial intelligence (AI) Disclosure: AI-assisted tools were used solely to improve language and readability and to generate a schematic illustration based on the authors' study protocol. No AI tool was used for the conception of the study, data generation, analysis, interpretation of results, or formulation of scientific conclusions. The authors reviewed, edited, and take full responsibility for the final manuscript.

REFERENCES

[1] Larsson L, Decker AM, Nibali L, Pilipchuk SP, Berglundh T, Giannobile WV. Regenerative medicine for periodontal and peri-implant diseases. J Dent Res. 2016;95(3):255-66. Available from: https://doi.org/10.1177/0022034515618887.

[2] Fakheran O, Fischer KR, Schmidlin PR. Enamel matrix derivatives as an adjunct to alveolar ridge preservation-a systematic review. Dent J (Basel). 2023;11(4):100. Available from: https://doi.org/10.3390/dj11040100.

[3] Reddy SSP, Francis DL, Thirumoorthi H, Rahul, Rathi M, Singh H, et al. Effectiveness of recombinant human bone morphogenetic protein-2 in socket preservation: A randomized controlled clinical and sequential human histological trial (BMP-2 TRIAL). Clin Exp Dent Res. 2025;11(3):e70134. Available from: https://doi.org/10.1002/cre2.70134.

[4] Dzobo K, Thomford NE, Senthebane DA, Shipanga H, Rowe A, Dandara C, et al. Advances in regenerative medicine and tissue engineering: Innovation and transformation of medicine. Stem Cells Int. 2018;2018:2495848. Available from: https://doi.org/10.1155/2018/2495848.

[5] Gu Z, Fu J, Lin H, He Y. Development of 3D bioprinting: From printing methods to biomedical applications. Asian J Pharm Sci. 2020;15(5):529-57. Available from: https://doi.org/10.1016/j.ajps.2019.11.003.

[6] Arumugam P, Kaarthikeyan G, Eswaramoorthy R. Three-dimensional bioprinting: The ultimate pinnacle of tissue engineering. Cureus. 2024;16(4):e58029. Available from: https://doi.org/10.7759/cureus.58029.

[7] Chen XB, Fazel Anvari-Yazdi A, Duan X, Zimmerling A, Gharraei R, Sharma NK, et al. Biomaterials / bioinks and extrusion bioprinting. Bioact Mater. 2023;28:511-36. Available from: https://doi.org/10.1016/j.bioactmat.2023.06.006.

[8] Tian S, Zhao H, Lewinski N. Key parameters and applications of extrusion-based bioprinting. Bioprinting. 2021;23:e00156. Available from: https://doi.org/10.1016/j.bprint.2021.e00156.

[9] Amirrah IN, Lokanathan Y, Zulkiflee I, Wee MFMR, Motta A, Fauzi MB. A comprehensive review on collagen type I development of biomaterials for tissue engineering: From biosynthesis to bioscaffold. Biomedicines. 2022;10(9):2307. Available from: https://doi.org/10.3390/biomedicines10092307.

[10] Fan L, Ren Y, Emmert S, Vučković I, Stojanovic S, Najman S, et al. The use of collagen-based materials in bone tissue engineering. Int J Mol Sci. 2023;24(4):3744. Available from: https://doi.org/10.3390/ijms24043744.

[11] Jeyachandran S, Aman M. Valorisation of fish scales and bones: A sustainable source of bioactive proteins and collagen for nutraceuticals. Bioresour Bioprocess. 2025;12(1):141. Available from: https://doi.org/10.1186/s40643-025-00970-w.

[12] Yamada S, Yamamoto K, Ikeda T, Yanagiguchi K, Hayashi Y. Potency of fish collagen as a scaffold for regenerative medicine. Biomed Res Int. 2014;2014:302932. Available from: https://doi.org/10.1155/2014/302932.

[13] Thirumalaivasan N. Collagen-composite scaffolds for alveolar bone and dental tissue regeneration: Advances in material development and clinical applications-a narrative review. Dent J (Basel). 2025;13(9):396. Available from: https://doi.org/10.3390/dj13090396.

[14] Yue C, Ding C, Xu M, Hu M, Zhang R. Self-assembly behaviour of collagen and its composite materials: Preparation, characterizations, and biomedical engineering and allied applications. Gels. 2024;10(10):642. Available from: https://doi.org/10.3390/gels10100642.

[15] Mondal S, Park S, Choi J, Vu TTH, Doan VHM, Vo TT, et al. Hydroxyapatite: A journey from biomaterials to advanced functional materials. Adv Colloid Interface Sci. 2023;321:103013. Available from: https://doi.org/10.1016/j.cis.2023.103013.

[16] Yang W, Han W, He W, Li J, Wang J, Feng H, et al. Surface topography of hydroxyapatite promotes osteogenic differentiation of human bone marrow mesenchymal stem cells. Mater Sci Eng C Mater Biol Appl. 2016;60:45-53. Available from: https://doi.org/10.1016/j.msec.2015.11.012.

[17] Zhu J. Bioactive modification of poly(ethylene glycol) hydrogels for tissue engineering. Biomaterials. 2010;31(17):4639-56. Available from: https://doi.org/10.1016/j.biomaterials.2010.02.044.

[18] Bellis SL. Advantages of RGD peptides for directing cell association with biomaterials. Biomaterials. 2011;32(18):4205-10. Available from: https://doi.org/10.1016/j.biomaterials.2011.02.029.

[19] Cernadas T, Ferreira M, Melo BL, de Melo-Diogo D, Correia IJ, Ferreira P, et al. UV-crosslinked biomaterials: Functionalized polyethylene glycol for tissue adhesive applications. Polymer. 2025;339:129189. Available from: https://doi.org/10.1016/j.polymer.2025.129189.

[20] Elango J, Zamora-Ledezma C. Rheological, structural, and biological trade-offs in bioink design for 3D bioprinting. Gels. 2025;11(8):659. Available from: https://doi.org/10.3390/gels11080659.

[21] Sangroniz L, Fernandez M, Santamaria A. Polymers and rheology: A tale of give and take. Polymer. 2023;271:125811. Available from: https://doi.org/10.1016/j.polymer.2023.125811.

[22] Upton A, Mylona A, Zimbitas G. Utilising design of experiment to design an optimised bioink for 3D bioprinting. J Mater Sci. 2025;60:10467-77. Available from: https://doi.org/10.1007/s10853-025-11076-1.

[23] Sun G, Zhang XZ, Chu CC. Effect of the molecular weight of polyethylene glycol (PEG) on the properties of chitosan-PEG-poly(N-isopropylacrylamide) hydrogels. J Mater Sci Mater Med. 2008;19(8):2865-72. Available from: https://doi.org/10.1007/s10856-008-3410-9.

[24] Elbadawi M. Rheological and mechanical investigation into the effect of different molecular weight poly (ethylene glycol)s on polycaprolactone-ciprofloxacin filaments. ACS Omega. 2019;4(3):5412-23. Available from: https://doi.org/10.1021/acsomega.8b03057.

[25] Liu X, Gaihre B, George MN, Miller AL, Xu H, Waletzki BE, et al. 3D bioprinting of oligo(poly[ethylene glycol] fumarate) for bone and nerve tissue engineering. J. Biomed Mater Res A. 2021;109(1):6-17. Available from: https://doi.org/10.1002/jbm.a.37002.

[26] Habib A, Sarah R, Tuladhar S, Khoda B, Limon SM. Modulating rheological characteristics of bio-ink with component weight and shear rate for enhanced bioprinted scaffold fidelity. Bioprinting. 2024;38:e00332. Available from: https://doi.org/10.1016/j.bprint.2024.e00332.

[27] Wu D, Yu Y, Tan J, Huang L, Luo B, Lu L, et al. 3D bioprinting of gellan gum and poly (ethylene glycol) diacrylate based hydrogels to produce human-scale constructs with high-fidelity. Mater Des. 2018;160:486-95. Available from: https://doi.org/10.1016/j.matdes.2018.09.040.

[28] Wenz A, Janke K, Weimer Nee Hoch E, Tovar G, Borchers K, Kluger P. Hydroxyapatite-modified gelatin bioinks for bone bioprinting. Bio Nano Materials. 2016;17(3). Available from: https://doi.org/10.1515/bnm-2015-0018.

[29] Bastos AR, Da Silva LP, Maia FR, Franco A, Noro J, Silva C, et al. Hydroxyapatite/alginate/gellan gum inks with osteoconduction and osteogenic potential for bioprinting bone tissue analogues. Int J Biol Macromol. 2024;271(Pt 2):132611. Available from: https://doi.org/10.1016/j.ijbiomac.2024.132611.

[30] Osidak EO, Kozhukhov VI, Osidak MS, Domogatsky SP. Collagen as bioink for bioprinting: A comprehensive review. Int J Bioprint. 2020;6(3):270. Available from: https://doi.org/10.18063/ijb.v6i3.270.

[31] Stepanovska J, Supova M, Hanzalek K, Broz A, Matejka R. Collagen bioinks for bioprinting: A systematic review of hydrogel properties, bioprinting parameters, protocols, and bioprinted structure characteristics. Biomedicines. 2021;9(9):1137. Available from: https://doi.org/10.3390/biomedicines9091137.
[32] Zhang T, Zhao W, Xiahou Z, Wang XW, Zhang K, Yin J. Bioink design for extrusion-based bioprinting. Applied Materials Today. 2021;25:101227. Available from: https://doi.org/10.1016/j.apmt.2021.101227.
[33] Charbe NB, Tambuwala M, Palakurthi SS, Warokar A, Hromić-Jahjefendić A, Bakshi H, et al. Biomedical applications of three-dimensional bioprinted craniofacial tissue engineering. Bioeng Transl Med. 2022;8(1):e10333. Available from: https://doi.org/10.1002/btm2.10333.

PARTICULARS OF CONTRIBUTORS:
1. Associate Professor, Department of Periodontics, Saveetha Dental College, Saveetha Institute of Medical and Technical Sciences, Saveetha University, Chennai, Tamil Nadu, India.
2. Undergraduate Student, Department of Periodontics, Saveetha Dental College, Saveetha Institute of Medical and Technical Sciences, Saveetha University, Chennai, Tamil Nadu, India.
3. Professor, Department of Periodontics, Saveetha Dental College, Saveetha Institute of Medical and Technical Sciences, Saveetha University, Chennai, Tamil Nadu, India.

NAME, ADDRESS, E-MAIL ID OF THE CORRESPONDING AUTHOR:
Dr. Parkavi Arumugam,
Associate Professor, Department of Periodontics, Saveetha Dental College, Saveetha Institute of Medical and Technical Sciences, Saveetha University, Chennai-600077, Tamil Nadu, India.
E-mail: parkavia.sdc@saveetha.com

PLAGIARISM CHECKING METHODS: [Jain H et al.]
- Plagiarism X-checker: Mar 19, 2026
- Manual Googling: Jul 04, 2026
- iThenticate Software: Jul 07, 2026 (1%)

ETYMOLOGY: Author Origin

EMENDATIONS: 6

AUTHOR DECLARATION:
- Financial or Other Competing Interests: None
- Was Ethics Committee Approval obtained for this study? Yes
- Was informed consent obtained from the subjects involved in the study? No
- For any images presented appropriate consent has been obtained from the subjects. No

Date of Submission: **Feb 27, 2026**
Date of Peer Review: **Apr 11, 2026**
Date of Acceptance: **Jul 09, 2026**
Date of Publishing: **Sep 01, 2026**